ADVANCED ENGINEERING MATERIALS

DOI: 10.1002/adem.200700320

Hierarchical ZnO Micro-/Nano-Structure Film**

By *Xiang Wu*, *Peng Jiang*,* *Wei Cai*, *Xue-Dong Bai*, *Peng Gao* and *Si-Shen Xie*

Design and construction of metal and semiconductor nanomaterials with complex multi-dimensional (MD) architectures are triggering a new tidal wave of research on self-organized growth of one-dimensional nanostructures. The realization of the hierarchical nanostructures can provide many potential opportunities for high technological applications in photonics, electronics, and magnetics as well as interface modification and advanced catalysis in engineering field. Recently, reports about branch-like metal[1] and urchin-like semiconductor complex nanostructures[2] have demonstrated a success in preparing the MD nanomaterials, but basic control mechanism and growth methods for new complex hierarchical nanostructures still remain open.

Zinc oxide (ZnO), a direct wide band gap (3.37 eV) semiconductor material with a large excitation binding energy (60 meV), has become one of the most important functional materials in parallel to carbon nanotubes since the discovery of ZnO nanobelts in 2001.[3] Unlike carbon nanotubes formed by rolling graphite layers, the formation of ZnO nanobelts or nanowires is mainly dominated by the preferential growth of the material along specific crystalline orientation. From the viewpoint of crystallography, ZnO crystal has the wurtzite structure with lattice parameters of $a = 0.3296$ and $c = 0.5206$ nm. It is a hexagonal phase with space group $P6_3mc$. The structure of ZnO can be depicted as a large number of alternating planes composed of tetrahedrally coordinated O^{2-} and Zn^{2+} ions, stacked alternatively along the *c*-axis. The oppositely charged ions produce positively charged (0001)-Zn and negatively charged (0001)-O polar surfaces, resulting in a normal dipole moment along the *c*-axis.[4] The intrinsic polarity is the origination of many special properties of ZnO such as piezoelectricity and spontaneous polarization as well as an important factor in understanding growth, etching and defect generation of the material. Due to three kinds of growing directions, i.e., <0001>, <0110> and <2110>, and ± (0001) polar-surface-induced phenomena, up to date, one has found various ZnO nanostructures such as nanowires,[5,6] nanotubes,[7] nanobelts,[8] nanocombs,[9] nanosaws,[10] nanohelices[11] and nanorings[12] *etc*. Recently, hierarchical ZnO nanostructures have attracted much attention. Zhang *et al.*[13] investigated the formation of tower-like ZnO submicron- and nano- structures by simply evaporating a mixture of Zn and Ga. Mo *et al.*[14] employed ethylenediamine-derived $Zn[en]_2^{2+}$ as a precursor to prepare curved MD ZnO nanorod structure with the shape of hollow microhemisphere. More recently, we also have realized the size control of ZnO nanowire or nanorod unit on curved surface in alkaline solution by using hydrothermal method. The one-dimensional ZnO nanounit grown on the curved surface exhibits a hexagonal cross-section profile with uniform body extending along c-axis direction.[15] In present study, we report another kind of new hierarchical ZnO micro-/nano-structure film constructed on metal Zn foil surface. This ZnO film is composed of a large quantity of urchin-like ZnO microspheres with bamboo-like ZnO branches shrinking in diameter gradually from micro- to nano-meter scale. The constructed interface material is expected to have potential multi-values in interface hydrophilic and hydrophobic modification, photocatalysis, and piezoelectric devices *etc*. The investigation also demonstrates that one can directly grow multi-dimensional ZnO micro/nano-structure thin film only by one-step thermal evaporation route.

Morphology and Structure of the Hierarchical ZnO Film

The hierarchical ZnO structure film was prepared by thermally evaporating a mixed powder of ZnS and graphite at 900 °C under low vacuum condition with the presence of residual oxygen. Morphology of as-synthesized product was firstly characterized by a field emission scanning electron mi-

[*] *Prof. W. Cai, X. Wu*
School of Materials Science and Engineering
Harbin Institute of Technology
Harbin 150001 (P. R. China)
E-mail: weicai@hit.edu.cn
Prof. P. Jiang, X. Wu
National Center for Nanoscience and Technology (NCNST)
No. 11, 1st North Street
Zhong-Guan-Cun, Hai-Dian District
Beijing 100080 (P.R.China)
E-mail: pjiang@nanoctr.cn
Prof. S. S. Xie, Prof. X. D. Bai, P. Gao
Institute of Physics
Chinese Academy of Sciences (CAS)
Beijing 100080 (P.R.China)
E-mail: ssxie@aphy.iphy.ac.cn

[**] *The work was financially supported by the National Natural Science Foundation of China (No.50772024), "973" National Key Basic Research Project (2003CB716900, 2005CB724700), Opening Research Foundation of the National Center for Nanoscience and Technology (NCNST), China.*

ADVANCED ENGINEERING MATERIALS

COMMUNICATIONS

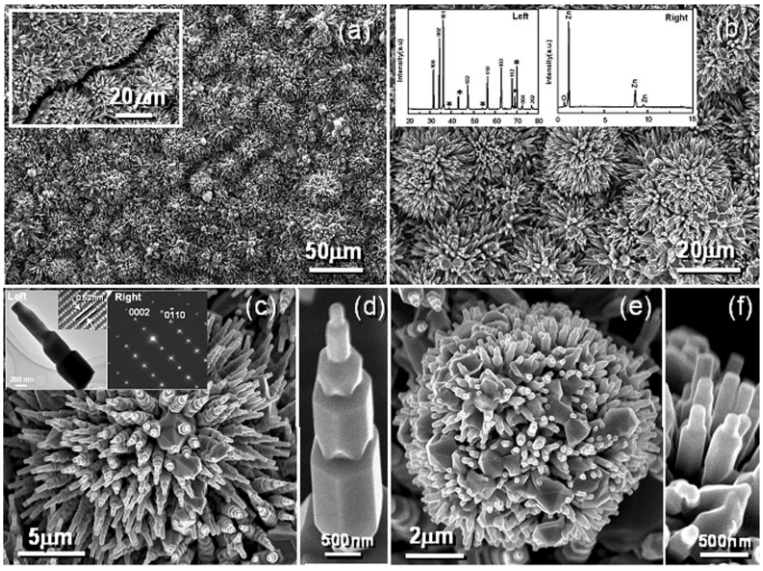

Fig. 1. FE-SEM images of the multi-dimensional urchin-like ZnO micro-/nano-structures with bamboo-like ZnO micro-/nano-wire branches formed on Zn substrate at higher temperature region (~ 500 °C). (a) A large-scaled morphology of the ZnO micro-/nano-structure film, insert showing a slit in the film, (b) a middle-scaled morphology of the product, insert showing XRD and EDS of the sample, (c) a high magnified SEM image of single urchin-like ZnO microsphere with longer branches, insert showing TEM images of a ZnO branch segment with a low and a high resolution and the corresponding diffraction pattern, (d) a typical bamboo-like ZnO micro-/nano-wire branch on the urchin-like ZnO microsphere, (e) a high magnified SEM image of individual urchin-like ZnO microsphere with shorter branches, (f) tower-like ZnO nanowire units formed on the ZnO microsphere.

croscopy (FE-SEM). Figure 1(a) demonstrates a typical low-magnified FE-SEM image of the Zn foil positioned at high temperature region (~ 500 °C). A large number of sphere-like microstructures distribute throughout the entire Zn substrate, insert shows a typical slit existing on the film. A closer view of these microspheres shows that they have an apparent urchin-like morphology with a diameter variation from several to several tens of micrometers (see Fig. 1(b)). High-magnification FE-SEM images reveal some structure details of these urchin-like architectures. One kind consists of longer bamboo-like micro-/nano-rods with an average length of 4 μm (see Fig. 1(c)). These rods are radially oriented with their growth axes pointing to center of the microsphere. Each rod is composed of several segments of short pillars. The pillars become thinner and thinner from the inner of the urchin-like microsphere to its outside, reducing in diameter from micro- to nano-meter scale. Each segment has a flat top and a bottom with regular-concave angles connecting with adjacent other segments (see Fig. 1(d)). Another kind comprises shorter tower-like nanorods with an average length of 600 nm. Some particles randomly intersperse among the nanorods on the microsphere surface (see Fig. 1(e) and 1(f)).

The powder X-ray diffraction (XRD) measurement of thus-obtained product demonstrates that most of diffraction peaks match well with wurtzite-type (hexagonal phase, space group $P6_3mc$) ZnO patterns (see insert (left) in Fig. 1(b)). Remnant weak diffraction peaks can be attributed to metal Zn, originating from un-oxidized Zn product or Zn foil substrate. Energy dispersive X-ray spectroscopy (EDS) analysis proves that only Zn and O elements exist in the product with a Zn/O molar ratio of ~ 1.1:1 (see insert (right) in Fig. 1(b)). No other element signals such as S, C, have been detected within the instrument detection limits, implying that ZnS has completely converted to Zn or ZnO by carbon thermal or oxidation reaction. Insert (left) and (right) in Figure 1(c) show transmission electron microscopy (TEM) images with a low and a high resolution as well as a selected area diffraction pattern recorded from a ZnO rod segment. The measured spacing from lattice fringes is about 0.52 nm along growth axis direction of the ZnO rod, being agreement with crystalline plane distance between two {0001}-type planes. These results reveal that the ZnO rod grows along [0001] direction with its side surface surrounded by {1010} facets.

To shed light on formation mechanism of these special MD ZnO architectures, more product morphologies have been examined by FE-SEM. The image in Figure 2(a) demonstrates a partly branched urchin-like microstructure, on which polyhedral particles with hexagonal section and step-like side faces can be clearly seen. The particles are probably Zn particle protrusions covered by ZnO shells. Small tower-like ZnO nanopillars have also been observed to extend out from top of the particles (see Fig. 2(b)). Note that some small ZnO nanopillars are also found to exist at side faces of the particles (see Fig. 2(c)). It seems that the nanopillars are grown from external Zn liquid droplets condensed on the particles, as shown in insert of Figure 2(c). Figure 2(d) shows a SEM image of a lower segment of a special bamboo-like ZnO micro-/nano-rod. {1010}-type side facet segments on the rod exhibit rhombic shape and arrange into necklace-like structure. Interestingly, the necklace-like ZnO structure also appears on inner facets of the microsphere (see Fig. 2(e) and 2(f)), implying that the ZnO structures probably nucleate and grow at different active sites on the Zn facets. In addition, other ZnO micro-/nano-structures with a corn-like morphology have also been found in the obtained product (see Fig. 2(g) and 2(h)).

To evaluate substrate effect, we used a same evaporation source and a Si(100) substrate instead of the Zn foil for preparation and deposition of product. Figure 3(a) shows a typical of low-magnified SEM image of the obtained product. Only tower-like ZnO structures with single, double and triple branches occur (see Fig. 3(b), 3(c) and 3(d)). No hierarchical ZnO film and microspheres exist on the Si substrate. It further indicates that the Zn foil substrate plays a critical role in supply of the rich Zn vapor, which favors the formation of the hierarchical ZnO film consisted of urchin-like ZnO microspheres.

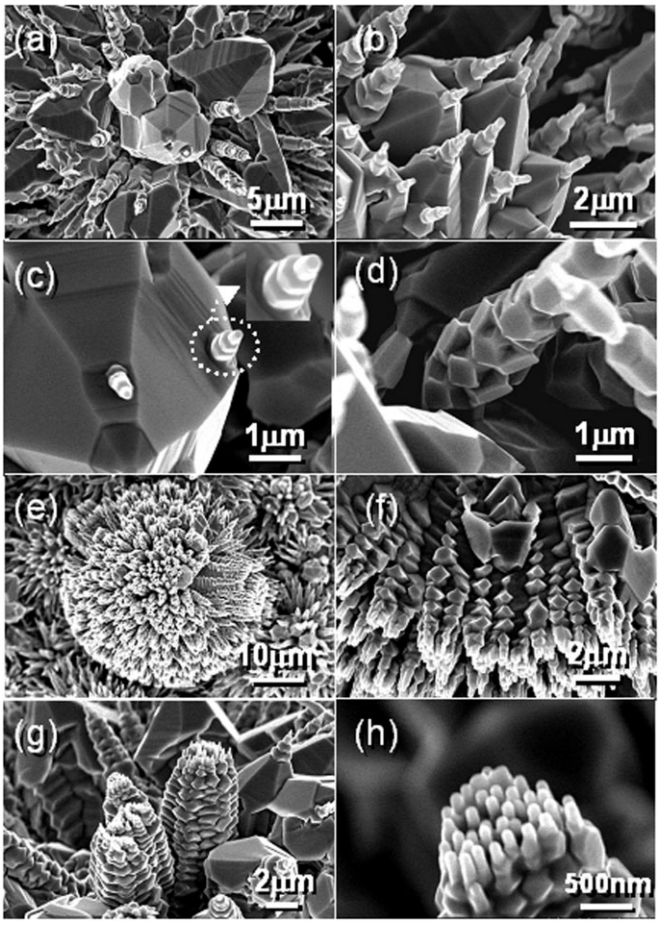

Fig. 2. FE-SEM images of partly branched urchin-like ZnO micro-/nano-structures. (a) A single urchin-like ZnO micro-/nano-structure on which some particle-like Zn protrusions covered by ZnO shell can be seen, (b) small tower-like ZnO tips grow out from the tops of the ZnO shell, (c) some extra small tower-like ZnO structures can also be formed on certain facets of polyhedral ZnO shells, insert shows a magnified image of a tower-like ZnO structure, (d) Root part of one special bamboo-like ZnO rod, demonstrating rhombus-shaped {1010} side facet segments of the rod and necklace-like structure, (e) A low resolution FE-SEM image of urchin-like ZnO micro-/nano-structure with a large gap, (f) In the urchin-like ZnO microsphere, some rhombus-shaped {1010} side facet segments are formed and arranged into necklace-like structure, (c) multi-tip corn-like ZnO branches, (d) On top of the ZnO corn, more ZnO nanorod tips can be found.

Growth Mechanism of the Hierarchical ZnO Nanostructures with Bamboo-like Branches

Based on the experimental observation, a possible formation mechanism of the MD ZnO structures can be proposed. It is worth noting that the hierarchical ZnO microstructure film has only been observed on the Zn foil located at higher temperature region (~ 500 °C). The temperature is much higher than melting point (419 °C) of metal Zn. At the temperature, surface of the Zn foil was firstly oxidized to form ZnO film by residual oxygen in quartz tube (see a slit of ZnO film on Zn substrate in insert of Fig. 1(a)). ZnO has a higher melting point (1975 °C) than metal Zn. Therefore, metal Zn under the ZnO film can sublime into vapor and overflow from gaps in the ZnO film. Combining with Zn vapor originated from carbon-thermal reduction of ZnS source, a large amount of Zn vapor exists above the Zn foil covered by a layer of ZnO film. The Zn vapor can condense again into larger individual metal Zn microspheres and smaller Zn microsphere aggregates on the ZnO-coated Zn substrate depending on its local vapor concentration. The suggestion can be further verified by SEM observation of the product collected at lower temperature region (~ 300 °C), where some individual larger Zn microspheres and aggregates of smaller microspheres can be found (see Fig. 4). Actually, at higher temperature than Zn melting point, surface of metal Zn microsphere probably is not smooth. From the viewpoint of crystal growth, the crystal morphology is dominated by the relative growth rate along various crystal plane orientations according to Bravais–Friedel law,[16] which explains that crystal growth along the high index crystal plane orientation is much faster than along low index plane orientation. For crystal Zn with wurtzite structure, growth rates along <0001>, <1010>, and <1011> directions are slower than those along other crystal plane directions. Therefore, on the surface of the Zn microspheres, some Zn polyhedral protrusions enclosed by {0001}, {1010}, and {1011} facets tend to be formed. ZnO facets with similar crystal plane index can be rapidly epitaxially produced by oxidization due to same wurtzite structure of Zn and ZnO, leading to polyhedral ZnO shell (see Fig. 2(a,b,c)). The large lattice mismatch between Zn and ZnO (~ 23.7 %) can induce gaps or pores on the ZnO shell due to strain induced by phase transformation. Part Zn sublimes out through the gaps or pores from inner Zn core, bringing on vacancies in the Zn core, which radially distribute from large to small towards center of the Zn core because more close to ZnO shell, more Zn are evaporated. As a result, urchin-like Zn core with coniform Zn needles are formed and are exposed to oxidize into ZnO. Because diameters of the Zn needles become thicker and thicker from outside to inner, formed ZnO rods also must exhibit similar morphology. In general, in the process of crystal growth, high index crystal planes have relative higher surface energy. Therefore, they are unstable. Only are some low index planes such as {1010}- and {0001}-type planes remained in final morphology. This is a possible reason why the bamboo-like ZnO branches are formed. Furthermore, in Figure 1(d), each ZnO pillar segment has a flat top and a bottom with six regular-concave angles. Figure 1(d) also shows several rhombic {1010} side facet segments of the forming ZnO rod. These further show that main bodies of the bamboo-like ZnO branches in the urchin-like ZnO MD structures are not produced by the growth of vapor-formed ZnO nuclei but are formed by oxidation of inner coniform Zn needles as well as further diffusion and fusion of formed ZnO.

Interestingly, we have also observed that some small ZnO towers with flat top are nucleated and grown on side facets and tops of polyhedral ZnO shells, as shown in Figure 2(b), 2(c) and Figure 2(h). In insert of Figure 2(c), a liquid-droplet-like base can be seen at the bottom of the ZnO tower. These tower-like ZnO structures are probably formed by nucleation,

ADVANCED ENGINEERING MATERIALS

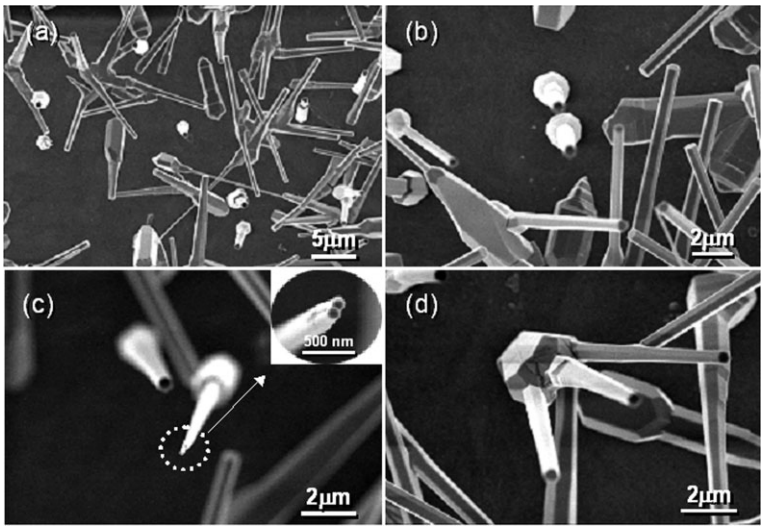

Fig. 3. FE-SEM images of ZnO product formed on Si(100) substrate. (a) A general morphology of the product, (b) tower-like ZnO microstructure, (c) tower-like ZnO microstructure with double branches, (d) ZnO microstructure with triple branches

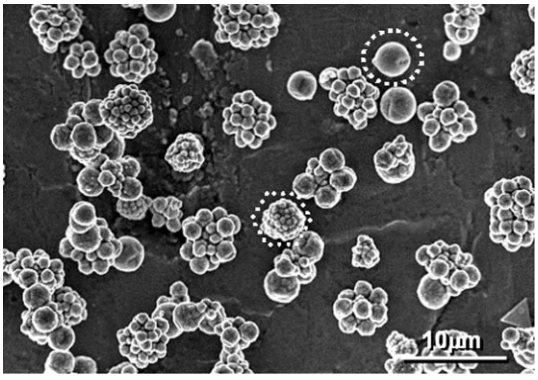

Fig. 4. FE-SEM images of the ZnO product obtained at lower temperature region (~ 300 °C). Some individual larger Zn microspheres and smaller microsphere aggregates randomly disperse on surface of the Zn substrate.

oxidation and growth of small Zn particles and tips. Formation mechanism of the tower-like ZnO structure is obviously different from what we have discussed above on main bodies of the bamboo-like ZnO branches. In the process, Zn vapor firstly condenses into Zn particles on surface of the ZnO shell, and then are further oxidized into ZnO nanoparticles. The ZnO nanoparticle can grow into larger ZnO prism enclosed by low energy crystal planes such as {1010}, {1011}, and {0001} by adsorbing vapor reactants. Shape of the ZnO prism is determined by relative competitive growth along various crystal plane orientations. For example, if growth rate along <1011> is far faster than along <0001>, hexagonal ZnO prism with a flat top can be produced. Contrarily, hexagonal ZnO prism with pyramid tip surrounded by six {1011}-type facets occurs. While growth rates along the two crystal plane orientations are comparable, hexagonal ZnO prism with truncated pyramid tip is final product. The size of flat (0001) facet on pyramid tip depends on little difference between growth rates along <0001> and <1011> direction. For present tower-like ZnO structure, one remarkable feature is that each hexagonal ZnO segment symmetrically positions on center of the flat top of nether ZnO base prism and has consistent crystal orientations with adjacent ZnO segments. It definitely shows that thinner hexagonal ZnO segment must grow out from small (0001) facet on top of truncated pyramid tip of hexagonal ZnO base prism in order to form the co-*c*-axial ZnO towers. In this case, obviously, growth rate along <0001> direction is a little bit faster than along <1011>. But following question is how to form ZnO tower structure? We think that second nucleation and growth of ZnO on top (0001) plane probably plays an important role. In general, it is believed that formation and evolution of islands on real crystalline surfaces are dominated by special relaxation mechanisms involved nucleation, surface diffusion, and diffusion over crystalline surface step edges.[17] When size of (0001) top plane achieves or is larger than the critical size for island nucleation, a new island can nucleate on the flat surface. Growth and shape of the new island depend on diffusion kinetics of adspecies. If adding adspecies deposited on the island experience a diffusion barrier (Ehrlich-Schwoebel barrier) over the island's edges, then next adspecie layer can nucleate before the old layer finishes so that a three-dimensional (3D) growth happens. Finally, a mound is formed. The mound can grow into new ZnO pillar but diameter is limited by top edges of the sloping side faces of the ZnO base prism due to existence of the diffusion barrier. Therefore, new ZnO pillar has absolute same crystal orientation as previous ZnO base prism. Once (0001) top surface of the new ZnO pillar reaches or is larger than the critical size for island nucleation, a new island nucleates again on the flat top surface. The process repeats step by step. With the increase of reaction time, each island can grow along three crystal orientations of <0001>, <1011>, and <1010>, forming a hexagonal segment bounded with six {1010} side facets. Finally, the tower-like ZnO structure can be formed.

Two possible formation processes for the bamboo-like and tower-like ZnO branches can be schematically demonstrated by Process I and II in Figure 5. According to suggested formation mechanisms, we can deduce that the hierarchical ZnO structure with longer bamboo-like ZnO branches is probably originated from the larger individual Zn microshpere (see Fig. 1(c)) while that with shorter tower-like ZnO nanorods results from smaller Zn microsphere aggregate (see Fig. 1(e)), because inner Zn core can rapidly use out for the smaller Zn microsphere, leaving a ZnO shell. ZnO can nucleate on the shell and grow into small tower-like ZnO branches.

Wettability, Room-temperature Raman and Photoluminescence Properties of the Hierarchical ZnO Nanostructures

Wettability of the Zn foil covered by a large amount of urchin-like hierarchical ZnO micro-/nano-structures has

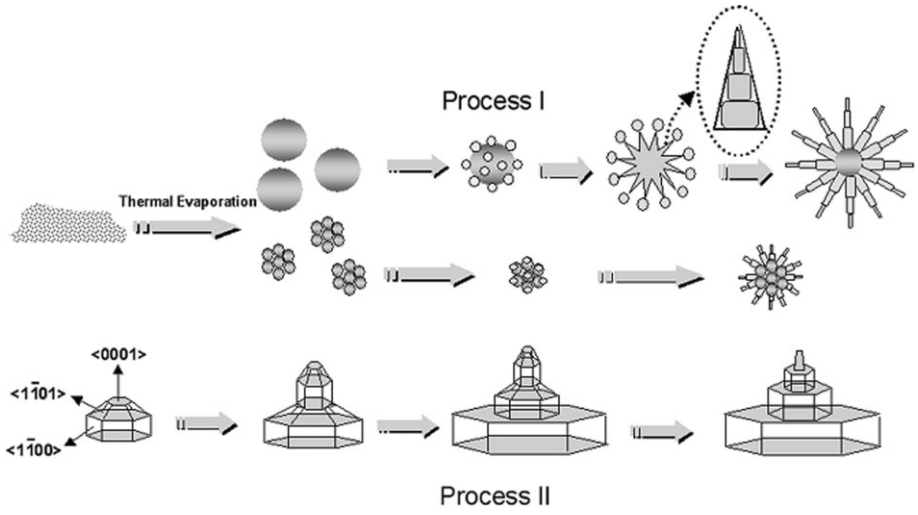

Fig. 5. A schematic illustration of possible growth processes of the bamboo-like ZnO nanowires formed on individual larger metallic Zn microsphere (Process I) and tower-like ZnO structures from smaller Zn particle and Zn microsphere aggregate (Process II).

been evaluated by the method of water contact angle (CA) measurement. The investigation will be helpful for one to find new route against corrosion of metal Zn bulk material owing to oxidization in air. Interestingly, the Zn foil modified by hierarchical ZnO exhibits a hydrophobic feature with a water CA of 128°. A typical photograph of the shape of a droplet of water on the film is shown in Figure 6(a). In contrast, the CA value of ZnO thin films constructed by using other routes such as spray pyrolysis is only 109°.[18] As is known, the wettability of solid substrates is mainly governed by their surface free energy and surface geometrical structure. In general, hydrophobic surface materials own lower surface free energy and large surface roughness.[19] Previous study on wettability of polypyrrole (PPy) material demonstrates that CA value of the PPy fabric can only reach 110° even though modified by fluorinated co-dopant with lower surface free energy.[20] Without modification by any surfactant with low surface energy, but CA value of the ZnO micro-/nano-structure surface can achieve 128°. This shows that it is the special rough surface structure to be responsible for the hydrophobic property. The hierarchical ZnO micro-/nano-structures on the Zn foil surface can ensure more air to be captured in the network structures, which can make hydrophobility of the Zn foil surface is remarkably improved.

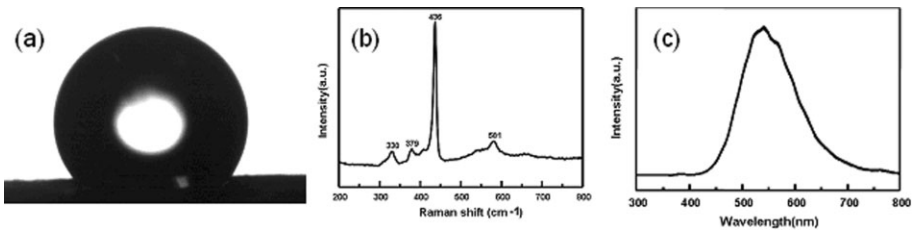

Fig. 6. (a) A photograph of water droplet contact angle for the Zn foil covered by the ZnO micro-/nano-structure film, (b) A room temperature Raman spectrum of the urchin-like ZnO micro-/nano-structure film, (c) A room temperature photoluminescence spectrum of the urchin-like ZnO micro-/nano-structure film grown on the Zn substrate.

Figure 6(b) demonstrates the Raman spectrum of the hierarchical ZnO nanostructures at room temperature. We can find four major vibration bands positioned at 330, 379, 436 and 581 cm^{-1}. In general, ZnO crystal with hexagonal wurtzite structure belongs to C_{6V}^4 ($P6_3mc$) space group. According to selection rule of phonon mode, Raman active modes for the wurtzite ZnO are: $A_1 + 2\,E_2 + E_1$.[21] Polar Symmetry A_1.and E_1 modes can split into the transverse optical (TO) and longitudinal optical (LO) phonon modes. E_2 mode is non-polar optical phonon mode, which is composed of two modes with low and high frequency. The bands centered at 379 and 581 cm^{-1} correspond to polar transverse A1 and longitudinal E1 optical phonon modes, respectively. The band at 436 cm^{-1} can be assigned to nonpolar optical phonon (E_2) mode of the ZnO micro-/nano-structures at high frequency, which is associated with oxygen deficiency. The peak at 330 cm^{-1} is attributed to the $2E_2$ mode. A strong intensity of the E_2 modes implies that thus-grown ZnO micro-/nano-structures are severely oxygen deficient at room temperature. In addition, stress induced in wurtzite crystals can obviously affect E_2 phonon frequency, for example, compressive stress can bring on an increase of the E_2 phonon frequency whereas tensile stress causes a decrease of the E_2 phonon frequency.[22] Therefore, the Raman scattering of the high frequency E_2 phonon is an indicator of residual stress within ZnO crystals. In the Raman spectrum of obtained ZnO nanostructures, the position of the E_2 (high) mode locates at 436 cm^{-1}, which is lower than the E_2 position (437 cm^{-1}) of the bulk ZnO standard Raman peak. This shows that a tensile stress remains in the ZnO nanostructures probably due to lattice distortion on ZnO micro-/nano-structure surface.

Figure 6(c) displays the room-temperature photoluminescence (PL) spectrum measured from thus-grown MD ZnO microstructures. A broad stronger green emission in the range of 425–700 nm (2.9–1.8 eV) and a much weaker ultraviolet emission centered at 375 nm (3.31 eV) occur. The former results from the recombination of the photon-generated holes with the electrons occupying the singly ionized oxygen vacancy, and the latter can be assigned to the emission from the free exciton under low excitation intensity.[23] The stronger green emission and the weaker UV band in the PL spectrum further verify that the MD ZnO microstructures have rich surface defect states, being very

ADVANCED ENGINEERING MATERIALS

COMMUNICATIONS

consistent to the result of Raman characterization. The surface defects are useful as effective photo-catalyst or sensitive biosensor active sites.

In summary, a kind of novel urchin-like hierarchical ZnO micro-/nano-structure film has been constructed on Zn foil by a simple one-step thermal evaporation process using a mixture of ZnS and graphite powder as a source. Individual ZnO micro-/nano-structures and bamboo-like or tower-like branches have been detailedly characterized by field-emission scanning electron microscope (FE-SEM) and high resolution transmission electron microscope (HRTEM). The results show different urchin-like ZnO structures probably originate from various Zn microshpere precursors. Reasonable formation mechanisms of the hierarchical ZnO micro-/nano-structures have been proposed on the base of obtained information. In addition, wettability, Raman and room-temperature photoluminescence properties of the ZnO micro-/nano-structure film have also been explored. These multi-branched ZnO assemblies are expected to have potential applications in protection of metal bulk Zn against corrosion in air as well as environmental friendly photo-catalysis.

Experimental

Urchin-like hierarchical ZnO micro-/nano-structure film was constructed on Zn foil substrate through a vacuum thermal evaporation process. In a typical preparation procedure, firstly, 1 g commercial-grade ZnS powder mixed with 1 g high-purified graphite powder was positioned in the center of a quartz tube in a single-zone horizontal tube furnace. Metal Zn foils serving as collectors were located in the quartz tube at the region away from the tube center along downstream direction. Then, the system was evacuated for 3 hrs to purge oxygen from the chamber. Subsequently, a mixed carrier gas of high-purified Ar with 5 % H_2 was flowed through the quartz tube at a rate of 50 standard cubic centimeters per minute. The furnace was heated up to 900 °C at a rate of 30 °C/min and kept at this temperature for 2 hrs. The gas pressure inside the tube was maintained at 300 Torr during the whole experiment. After the furnace was naturally cooled to room temperature, Surfaces of Zn foils positioned on certain temperature regions was found to become white color. Crystalline phase structure of thus-synthesized products was examined by using powder X-ray diffraction (XRD, Rigaku D/MAX2000 x-ray diffractometer with CuKα (λ=1.5418 Å)). The morphology and local crystal structure of the product were further characterized by a field-emission scanning electron microscope (FE-SEM, Hitachi S-4800) equipped with an energy-dispersion X-ray detector (EDX, INCA300) and a high-resolution transmission electron microscope (HRTEM, JEOL JEM-2010). Water contact angles (CAs) of the hierarchical ZnO film were measured by using a Dataphysics OCA20 contact angle system at ambient temperature. The CA value was obtained by averaging CA values measured at three different positions on the same sample. For Raman spectrum investigation of the ZnO film, a Renishaw microspectrometer (RM2000) with a 3600 grooves/mm grating in the backscattering configuration was employed. An Ar^+ ion laser (λ = 514.5 nm) was used as an excitation source. Photoluminescence (PL) spectrum was recorded at room temperature using a He-Cd laser with a wavelength of 325 nm as an excitation light source.

Received: November 19, 2007
Final version: December 24, 2007
Published online: April 15, 2008

[1] M. B. Osman, H. W. Benjamin, S. Francesco, *Chem. Mater.* **2006**, *18*, 3297.
[2] B. Liu, H. C. Zeng, *J. Am. Chem. Soc.* **2004**, *126*, 16744.
[3] Z. W. Pan, Z. R. Dai, Z. L. Wang, *Sci.* **2001**, *291*, 1947.
[4] Z. L. Wang, X. Y. Kong, Y. Ding, P. X. Gao, W. Hughes, R. S. Yang, Y. Zhang, *Adv. Funct. Mater.* **2004**, *14*, 943.
[5] C. M. Lieber, Z. L. Wang, *MRS Bull.* **2007**, *32* , 99.
[6] P. Jiang, J. J. Zhou, H. F. Fang, C. Y. Wang, S. S. Xie, *Mater. Lett.* **2006**, *60*, 2516.
[7] H. D. Yu, Z. P. Zhang, M. Y. Han, X. T. Hao, F. R. Zhu, *J. Am. Chem. Soc.* **2005**, *127*, 2378.
[8] Z. L. Wang, *Annu. Rev. Phys. Chem.* **2004**, *55*, 159.
[9] Z. L. Wang, X. Y. Kong, J. M. Zuo, *Phys. Rev. Lett.* **2003**, *91*, 185502.
[10] H. J. Fan, R. Scholz, A. Dadgar, A. A. Krost, M. Zacharias, *Appl. Phys. A* **2005**, *80*, 457.
[11] P. X. Gao, Y. Ding, W. J. Mai, W. L. Hughes, C. S. Lao, Z. L. Wang, *Sci.* **2005**, *309*, 1700.
[12] X. Y. Kong, Y. Ding, R. S. Yang, Z. L. Wang, *Sci.* **2004**, *303*, 1348.
[13] Y. Liang , X. T. Zhang, L. Qin, E. Zhang, H. Gao, Z. G. Zhang, *J. Phys. Chem. B* **2006**, *110*, 21593.
[14] M. S. Mo, J. C. Yu, L. Z. Zhang, S. K. A. Li, *Adv. Mater.* **2005**, *17*, 756.
[15] P. Jiang, J. J. Zhou, H. F. Fang, C. Y. Wang, Z. L. Wang, S. S. Xie, *Adv. Funct. Mater.* **2007**, *17*, 1303.
[16] J. D. H. Donnay, D. Harker, *Am. Mineral.* **1937**, *22*, 446.
[17] W. C. Elliot, P. F. Miceli, T. Tse, P. W. Stephens, *Phys. Rev. B* **1996**, *54*, 17938.
[18] R. D. Sun, A. Nakajima, A. Fujishima, T. Watanabe, K. Hashimoto, *J. Phys. Chem. B* **2001**, *105*, 1984.
[19] X. F. Gao, L. Jiang, *Nature* **2004**, *432*, 36.
[20] D. Mecerreyes, V. Alvaro, I. Cantero, M. Bengoetxea, P. A. Calvo, H. Grande, J. Rodriguez, J. A. Pomposo, *Adv. Mater.* **2002**, *14*, 749.
[21] T. C. Damen, S. P. S Porto, B. Tell, *Phys. Rev.* **1966**, *142*, 570.
[22] M. Kubal, *Surf. Interface Anal.* **2001**, *31*, 987.
[23] K. Vanhusden, C. H. Seager, W. L. Warren, D. R. Tallant, J. A. Voigt, *Appl. Phys. Lett.* **1995**, *68*, 403.

